Chapter 3

Intracellular storage and regulated secretion of von Willebrand factor in quantitative von Willebrand disease

Jiong-Wei Wang, Karine M. Valentijn, Hetty C. de Boer, Richard J. Dirven, Anton Jan van Zonneveld, Abraham J. Koster, Jan Voorberg, Pieter H. Reitsma and Jeroen Eikenboom

Adapted from *J Biol Chem. 2011 Jul; 286(27): 24180-24188*

Summary

Background: Several missense mutations in the von Willebrand Factor (VWF) gene of von Willebrand disease (VWD) patients have been shown to cause impaired constitutive secretion and intracellular retention of VWF. However, the effects of those mutations on the intracellular storage in Weibel-Palade bodies (WPB) of endothelial cells and regulated secretion of VWF remain unknown.

Methods and results: We demonstrate, by expression of quantitative VWF mutants in HEK293 cells, that four missense mutations in the D3 and CK-domain of VWF diminished the storage in pseudo-WPB, and led to retention of VWF within the endoplasmic reticulum (ER). Immunofluorescence and electron microscopy data showed that the pseudo-WPB formed by missense mutant p.Cys1060Tyr are indistinguishable from those formed by normal VWF. p.Cys1149Arg, p.Cys2739Tyr and p.Cys2754Trp formed relatively few pseudo-WPB which were often short and sometimes round rather than cigar-shaped. The regulated secretion of VWF was impaired slightly for p.Cys1060Tyr but severely for p.Cys1149Arg, p.Cys2739Tyr and p.Cys2754Trp. Upon co-transfection with wild type VWF, both intracellular storage and regulated secretion of all mutants were (partly) corrected.

Conclusions: In conclusion, defects in the intracellular storage and regulated secretion of VWF following ER retention may be a common mechanism underlying VWD with a quantitative deficiency of VWF.

Introduction

The hemostatic protein von Willebrand factor (VWF) plays important roles in hemostasis by facilitating platelet adhesion to injured endothelium and by carrying coagulation factor VIII (FVIII) in order to protect it from rapid proteolytic inactivation [1]. A defect in VWF leads to the most common inherited human bleeding disorder, von Willebrand disease (VWD) [2]. VWD is classified into 3 types: types 1 and 3 are quantitative VWD characterized by defects that result in a partial (type 1) or virtually complete (type 3) deficiency of VWF in plasma; type 2 VWD is caused by defects that result in qualitatively different VWF with abnormal function [2]. Among all the index cases, type 1 VWD is the most common form. Missense mutations compose the majority of mutations causing type 1 VWD (up to 75%), but only a minority of the mutations causing type 3 VWD [3-6]. In the latter cases nonsense mutations and deletions predominate.

VWF is synthesized as a precursor protein containing a signal peptide (22-amino acids), an N-terminal propeptide (D1 and D2 domains, 741 amino acids) and a mature peptide comprising multiple domains (D'-D3-A1-A2-A3-D4-B1-B2-B3-C1-C2-CK, 2050 amino acids) [7]. Following its synthesis in the endoplasmic reticulum (ER) proVWF (after cleavage of the signal peptide) dimerizes via formation of intermolecular disulfide bridges in the cysteine knot (CK) domain [1]. ProVWF dimers are transported to the Golgi apparatus; in this compartment propeptide-mediated assembly of multimers occurs through formation of intermolecular disulfide bridges within the D'D3 domains [1]. Processing of proVWF presumably by furin occurs in the *trans*-Golgi network. In the same compartment, VWF is either secreted constitutively or tubulized and packaged into Weibel-Palade bodies (WPB) for basal and regulated secretion [1,8,9]. After stimulation, high molecular weight (HMW) VWF multimers released from WPB rapidly form platelet-catching VWF filaments on the endothelial surface [10]. Quantitative or qualitative defects in assembly of HMW VWF multimers contribute to the bleeding tendency in VWD [11-13].

Ectopic expression of VWF in non-endothelial cell lines, like HEK293, leads to the formation of so-called pseudo-WPB that resemble WPB in endothelial cells [14-17]. Such cell-line models have been proven useful for the study of VWF and e.g. led to the discovery that the non-covalent interaction between the propeptide (D1-D2 domains) and the D'-D3-A1 domains of VWF is essential for tubulation and storage of VWF into WPB [18,19].

Missense mutations in VWF have been identified in quantitative as well as

qualitative VWF defects. We and others have shown that the missense mutations that cause quantitative VWD (type 1 and 3) impair constitutive secretion of VWF [20-30]. However, the effects of such mutations on WPB formation, VWF tubulation and regulated WPB secretion remain unknown. Moreover, the effects of type 1/3 VWD-causing VWF mutations on the formation and secretion of WPB have been neglected in most studies. The aim of our study was to elucidate whether quantitative VWF deficiencies in VWD are due to ER retention and/or lack of WPB formation, or accompanied by the formation of morphologically abnormal WPB that led to a malfunctioning (regulated) secretion of VWF.

We have studied quantitative VWF missense mutations in HEK293 cells: p.Cys1060Tyr and p.Cys1149Arg in the D3 domain that may affect the non-covalent interaction between the propeptide and mature VWF, and p.Cys2739Tyr and p.Cys2754Trp in the CK-domain that interfere with dimerization of VWF. Based on our results, we propose a common pathogenic mechanism for VWD with quantitative deficiencies of VWF.

Materials and methods

Patients and mutations

The mutations investigated in this study were originally identified in VWD patients. The mutation in exon 24, c.3179G>A, causes a cysteine substitution into tyrosine (p.Cys1060Tyr) and was identified in a heterozygous type 1 VWD participant of the MCMDM-1VWD study [31]. p.Cys1149Arg was identified in heterozygous type 1 VWD patients with moderately severe bleeding tendencies and was reported before [20]. p.Cys2739Tyr was described in a compound heterozygous type 3 VWD patient with the other allele carrying a premature stop codon [32]. p.Cys2754Trp was identified in a homozygous type 3 VWD patient [33].

Plasmid constructs – Recombinant pSVH expression plasmids containing full length cDNAs encoding either wild-type human VWF (WT-VWF) or p.Cys1149Arg, p.Cys2739Tyr and p.Cys2754Trp VWF variants have been described before [23]. The full length VWF cDNA fragments, obtained by EcoRI restriction of these pSVH-VWF plasmids, were cloned into the pCI-neo mammalian expression vector (Promega, Madison, WI, USA). Mutation p.Cys1060Tyr was introduced into pCI-neo WT-VWF plasmid with the QuikChange XL Site-Directed Mutagenesis Kit (Stratagene, La Jolla, CA, USA).

Cell culture and transfection

HEK293 cells were purchased from the ATCC (Rockville, USA) and cultured in Minimum Essential Medium α Medium (α-MEM, Invitrogen, Carlsbad, CA, USA) supplemented with 10% fetal calf serum, 50 μg/mL gentamicin (Invitrogen). Human umbilical vein endothelial cells (HUVECs) were obtained as described previously [34] and cultured in EGM-2 medium (Lonza, Breda, The Netherlands) supplemented with 100 U/mL penicillin, 100 μg/mL streptomycin and 250 ng/mL amphotericin (Invitrogen). HEK293 cells were seeded and 24 hours later transfected using FuGENE HD transfection reagent (Roche Diagnostics, Mannheim, Germany) according to the manufacturer's instructions. For transient transfection, the growth medium was refreshed 24 hours after transfection, and cells were grown for another 48 hours before analysis (which means 72 hours after the actual transfection). All the data in the present study were collected 72 hours post transfection unless otherwise stated. The stably transfected cells were selected by G418 (Invitrogen) for 3~5 weeks.

Immunofluorescence analysis

HEK293 cells were seeded on 1% gelatin pre-coated glass cover slips in 24-well plates. Cells were fixed 72 hours post transfection with 4% paraformaldehyde in 0.1 M phosphate buffer (pH 7.4) for 30 minutes on ice. Cells were rinsed with 50 mM Tris-HCl (pH 7.4), and permeabilized with 0.02% saponin (Sigma-Aldrich, St. Louis, MO, USA) in phosphate buffer (pH 7.4) for 20 minutes at room temperature. Following 10 minutes blocking with 5% normal goat serum (DAKO, Glostrup, Denmark), cells were incubated with first antibodies and then with fluorescence conjugated secondary antibodies. Monoclonal antibody CLB-RAg35 was used to visualize VWF [35]. Polyclonal rabbit anti-human Protein Disulfide Isomerase (PDI) antibody A66 (obtained from Prof. I. Braakman, Department of Chemistry, Utrecht University, Utrecht, The Netherlands) was used to visualize the ER [36]. Monoclonal anti-GM130 (BD Biosciences, California, USA) and polyclonal rabbit anti-human TGN46 (Sigma-Aldrich) were used to visualize *cis*- and *trans* Golgi networks, respectively. Monoclonal mouse anti-LAMP1 (mAb BB6; kindly provided by Dr. S. Carlsson, Umeå, Sweden) was used to visualize lysosomes [37]. Alexa 488- and Alexa 594-conjugated secondary antibodies were purchased from Invitrogen. Cells were embedded by Aqua-Poly/Mount medium (Polysciences, GmbH, Germany) and analyzed by Leica SL confocal laser scanning microscopy with a 63X/1.40 NA oil objective. To quantify pseudo-WPB, 150~300 VWF positive

cells from 2 independent experiments were randomly selected and analyzed. We used similar morphological criteria as reported by Michaux et al [17]. Briefly, we categorized the VWF positive but PDI negative granules as pseudo-WPB based on the immunofluorescent staining, and the pseudo-WPB with a ratio of length over diameter <2 as "round pseudo-WPB" and those with a ratio ≥2 as "elongated pseudo-WPB". To quantify the ER retention of VWF, cells were divided into three categories: the cells with all VWF co-stained with PDI as "ER", the cells with pseudo-WPB only but no ER retention as "WPB" and the cells with pseudo-WPB and ER retention as "WPB+ER".

Electron microscopy

HEK293 cells were seeded on 35 mm Petri dishes and fixed 72 hours post transfection (overnight at 4°C) with 2% paraformaldehyde and 2% glutaraldehyde in 0.1 M phosphate buffer (pH 7.4). Cells were then prepared for electron microscopy as previously described [38]. Briefly, cells were post-fixed for 60 minutes with 1% osmium tetroxide and for 30 minutes with 1% tannic acid. The samples were then dehydrated with serial concentrations of ethanol and embedded in Epon. 70-100 nm sections were cut by means of a Leica Ultracut UC6 microtome and placed on carbon and formvar-coated copper grids (one slot). Sections were stained with uranyl acetate and lead citrate, and then visualized with a Tecnai 12 at 120 kV equipped with a 4kx4k CCD camera (Model Eagle, Fei Company, The Netherlands).

Basal and regulated secretion

For the basal secretion, the conditioned media and cell lysates were collected 72 hours post transfection. To study the regulated secretion of VWF, 72 hours post transfection cells were rinsed twice with pre-warmed release medium (OPTIMEM1 medium, 10 mM HEPES [N-2-hydroxyethylpiperazine-N'-2-ethanesulfonic acid], 0.2% bovine serum albumin, pH 7.4) and incubated for 60 minutes with the release medium in the absence or presence of phorbol-12-myristate-13-acetate (PMA) (Sigma-Aldrich) at a final concentration of 160 nM. The media were collected for the assay of secreted VWF. To quantify intracellular VWF, cells were rinsed and then lysed overnight at 4°C in Passive Lysis Buffer (PLB, Promega) supplemented with the protease inhibitor cocktail Complete™ with EDTA (Roche). Cell lysates were collected and vortexed for 10 seconds. All the media and cell lysates were centrifuged for 5 minutes at 14,000*g*. The supernatants were supplemented with

phenylmethylsulfonyl fluoride (PMSF) (Roche) at a final concentration of 100 µM, and then analyzed immediately or snap-frozen. VWF:Ag was measured by ELISA as previously described [23]. To calculate the regulated secretion of VWF during stimulation, secreted VWF was expressed as a fraction of total VWF (% of total = absolute VWF:Ag in the medium/(absolute VWF:Ag in the medium + absolute VWF:Ag in the cell lysate) × 100).

Western blot analysis of VWF – Seventy-two hours post transfection the growth medium was replaced with release medium (see above). Twenty-four hours later, the conditioned media and cell lysates were collected as described above. VWF multimers were analyzed by non-reducing 1.6% agarose gel electrophoresis with sodium dodecyl sulfate (SDS) followed by Western blot as described [23]. To analyze subunit-composition of VWF, samples were reduced by incubation at 95°C for 5 minutes in sample buffer containing 20 mM dithiothreitol and separated on Novex 4% Tris-Glycine gel (Invitrogen). Reduced VWF was immunostained with polyclonal rabbit anti-human VWF conjugated to horseradish peroxidase (DAKO) and visualized with Supersignal WestFemto (Thermo Scientific, Rockford, IL, USA).

Results

Basal secretion of VWF variants

Basal secretion of VWF variants was investigated in transiently transfected HEK293 cells. The amount of VWF:Ag in medium or lysate is shown in Table 1. Compared to WT-VWF, secretion of p.Cys1060Tyr in the medium was decreased (<65% of WT-VWF), whereas the secretion of the other three variants was more severely impaired (<15% of WT-VWF). There was almost no detectable secretion of the p.Cys1149Arg and p.Cys2739Tyr mutated proteins. The readily detectable presence of p.Cys1149Arg and p.Cys2739Tyr proteins in the cell lysates indicated that those mutants were in fact synthesized but retained intracellularly. The total absolute amount of VWF:Ag measured in medium and lysate, however, was decreased. As no VWF was detectable by immunofluorescent staining in lysosomes or the Golgi apparatus (data not shown), the VWF mutants may have been degraded via the proteasome-associated pathway that has been implicated in the degradation of p.Cys1149Arg in an earlier study [39].

To mimic heterozygosity, co-transfections were performed with WT-VWF (Table 1). The secretion of VWF after p.Cys1060Tyr/WT co-transfection was close to WT-VWF only, and in the case of p.Cys1149Arg/WT, p.Cys2739Tyr/WT and p.Cys2754Trp/WT co-transfections yielded levels of about 40-65% of WT-VWF.

Intracellular distribution of VWF in transfected HEK293 cells

The intracellular localization of VWF in transfected HEK293 cells was analyzed with confocal immunofluorescence microscopy by co-staining of VWF and the ER marker PDI. Upon transfection HEK293 cells formed VWF storage vesicles, so-called pseudo-WPB that resemble WPB in endothelial cells (Figures 1A, 2A-B) [17]. Seventy-two hours post transfection almost all cells that expressed WT-VWF stored VWF in elongated pseudo-WPB (Figure 1A). Granular staining (non-overlapping with PDI) resembling pseudo-WPB was observed to a varying extent for the four VWF mutants p.Cys1060Tyr, p.Cys1149Arg, p.Cys2739Tyr and p.Cys2754Trp (Figure 1B-E). The pseudo-WPB formed by p.Cys1060Tyr were indistinguishable from those formed by WT-VWF (Figure 1B). The pseudo-WPB formed by the other mutants, p.Cys1149Arg, p.Cys2739Tyr and p.Cys2754Trp were shorter and often round (Figure 1C-E). Compared to WT-VWF and p.Cys1060Tyr, mutations p.Cys1149Arg, p.Cys2739Tyr and p.Cys2754Trp led to retention of much of the produced VWF in the ER (Figure 1A-E). Upon co-transfection with WT-VWF (Figure 1F-I), the impaired storage of VWF variants was corrected to a variable extent with the majority of cells containing VWF in both pseudo-WPB and ER.

Table 1. Expression of VWF variants in transfected HEK293 cells

Variant	Transfection	VWF:Ag* Medium		VWF:Ag* Lysate	
		mU	%	mU	%
WT-VWF		92.5 ± 3.7	100	38.2 ± 5.6	100
p.Cys1060Tyr	Single transfection	57.4 ± 1.8	62.3 ± 4.2	37.9 ± 10.5	96.3 ± 13.7
	Co-transfection	80.7 ± 7.2	88.0 ± 10.9	39.1 ± 2.0	104.9 ± 8.8
p.Cys1149Arg	Single transfection	2.7 ± 1.5	3.1 ± 1.6	51.2 ± 10.8	139.1 ± 38.3
	Co-transfection	39.7 ± 2.0	43.2 ± 3.9	56.3 ± 2.7	151.6 ± 16.3
p.Cys2739Tyr	Single transfection	0.5 ± 0.3	0.7 ± 0.4	34.1 ± 6.5	88.8 ± 8.2
	Co-transfection	52.1 ± 2.8	56.8 ± 5.4	39.1 ± 3.2	104.5 ± 9.5
p.Cys2754Trp	Single transfection	11.4 ± 1.3	12.3 ± 1.0	43.0 ± 6.5	113.2 ± 9.4
	Co-transfection	58.4 ± 6.2	63.9 ± 9.5	47.9 ± 1.7	129.4 ± 14.4

*VWF:Ag (mU) was produced by about 7×10^5 cells in the medium or lysate. In parallel, VWF:Ag is expressed as percentage relative to the amount of VWF:Ag in the medium and lysate of cells expressing WT-VWF. Each value represents the mean ± SEM of three independent experiments in duplicate. Co-transfections were in a 1:1 ratio with WT-VWF cDNA.

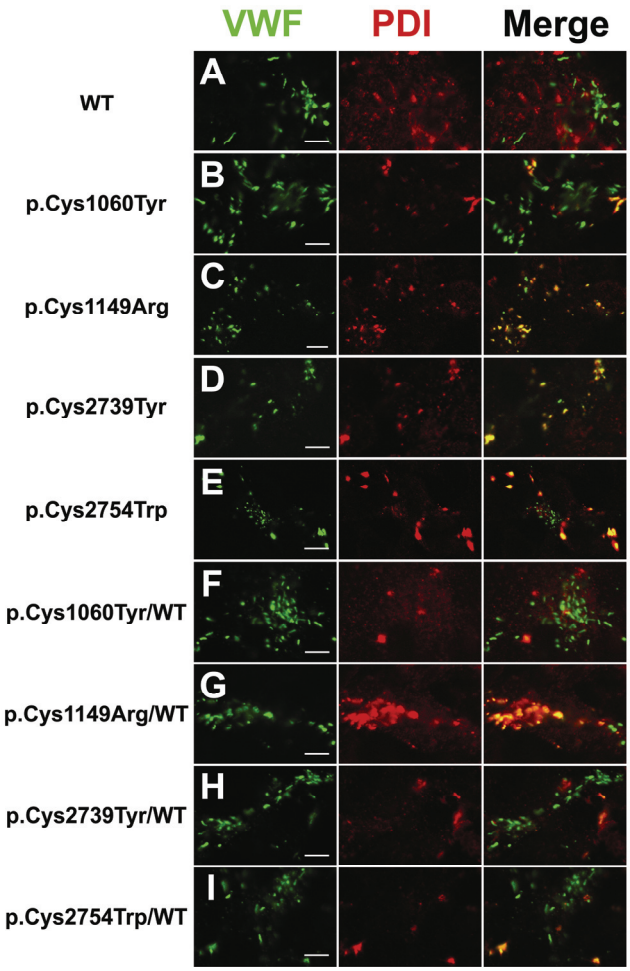

Figure 1. Intracellular distribution of WT-VWF and variants in transfected cells. HEK293 cells were fixed for immunofluorescence imaging 72 hours after single transfection (A-E) or co-transfection of VWF variants with WT-VWF (F-I). Fixed cells were stained for VWF (green channel, left panel) and for PDI (ER marker, red channel, middle panel). In the right panel (merge of green and red channels), the pseudo-WPB show up in green (VWF staining only) and the ER containing VWF shows up in yellow as a result of double staining with ER marker PDI. Scale bars = 5 μm.

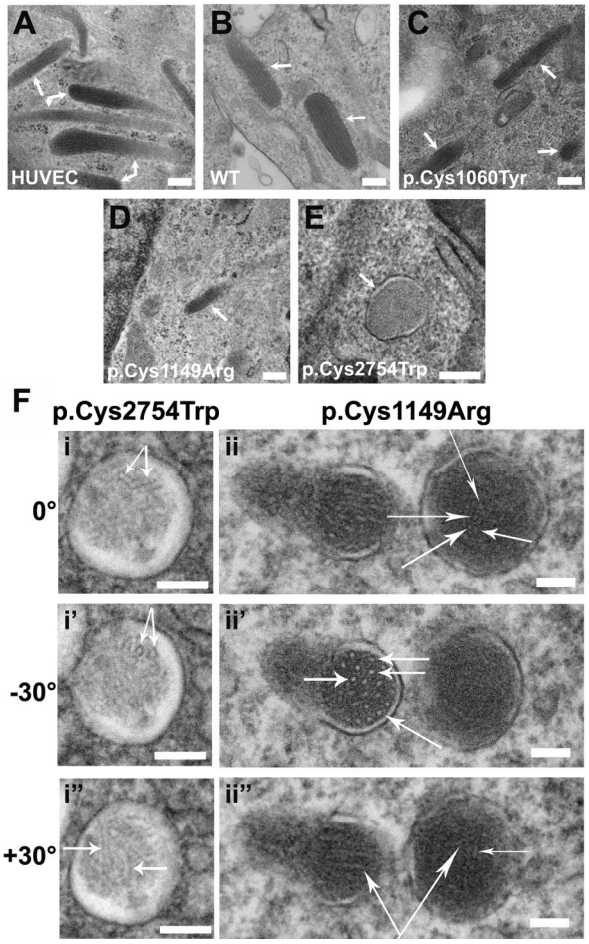

Figure 2. (Pseudo-) WPB visualized by TEM. HUVECs were fixed and analyzed with TEM (A). HEK293 cells were fixed 72 hours post transfection with WT-VWF (B), p.Cys1060Tyr (C), p.Cys1149Arg (D), or p.Cys2754Trp (E and F i-i") and analyzed with TEM. In p.Cys2754Trp transfected cells, the majority of storage vesicles are round (E). The presence of tubular structures inside the round vesicles was confirmed by tilting the sections (F). In panel F, HEK293 cells transiently expressing p.Cys2754Trp or stably expressing p.Cys1149Arg were analyzed with TEM. The sample is 100 nm thick and visualized at 0° tilt (i, ii), minus 30° tilt (i', ii') or plus 30° tilt (i'', ii''). Note in p.Cys2754Trp one short hinged tubule indicated by arrows (i), two transverse tubules (hollow rings, i') and two short longitudinal (vertical) tubules (i''). In p.Cys1149Arg, the transversally sectioned tubules (rings) are indicated by arrows in the right pseudo-WPB (ii) and in the left pseudo-WPB (ii'). By tilting the stage +30°, two short longitudinal tubules appeared in the right pseudo-WPB and some longer tubules in the left one (indicated by arrows in ii''). The relatively fewer and shorter tubules in the round pseudo-WPB suggest the storage of VWF in disarray. In panels A-E, scale bars = 200 nm; in panel F, scale bars = 100 nm.

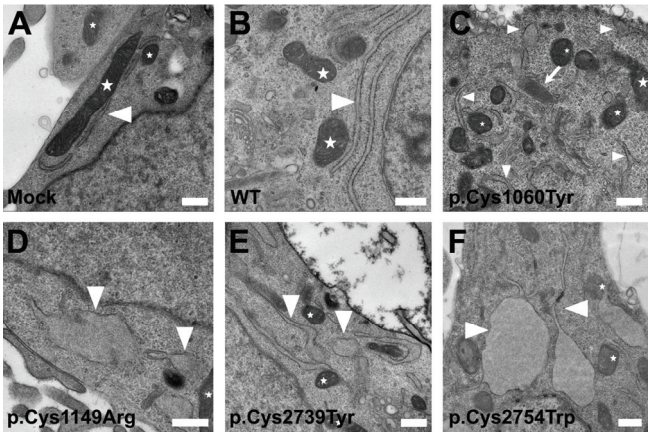

Figure 3. ER visualized by TEM. HEK293 cells were fixed and analyzed as in Figure 2. The morphology of the ER is normal in mock (A) or WT-VWF transfected cells (B), but dilated ER was observed in the cells following expression of each of the five mutants (C-F). Note the grossly dilated ER with thin tails in panel F. The arrows, arrowheads and stars indicate the pseudo-WPB, ER and mitochondria, respectively (panels A-F). Scale bars = 500 nm.

These observations were further confirmed by transmission electron microscopy (TEM). In WT-VWF transfected cells, elongated and electron dense pseudo-WPB were observed with internal striations, indistinguishable from those found in endothelial cells (Figure 2A-B). Pseudo-WPB were also observed in the cells following expression of each of the VWF mutants (Figure 2C-E) except for mutant p.Cys2739Tyr for which we were not able to visualize with certainty organelles with internal tubules. In accordance with the light microscopical data, most of the pseudo-WPB observed in the cells expressing mutants were much shorter than those in WT-VWF transfected cells. Strikingly, in the p.Cys2754Trp transfected cells the majority of VWF storage vesicles visualized by TEM were rather round instead of elongated (74 of 80 pseudo-WPB are round, i.e. 93%) (Figure 2E and supplemental Figure S1C). In contrast, 4 out of 47 pseudo-WPB (i.e. 9%) were round for WT-VWF. Those round vesicles reflect pseudo-WPB as they contain disorganized tubular structures which suggest the storage of VWF tubules, as shown by tilting the sample (Figure 2F i-i"). Similar round shaped pseudo-WPB were also observed in p.Cys1149Arg transfected cells, although to a lesser extent (7 of 24, i.e. 29%). Furthermore, grossly dilated ER was observed in many cells expressing the VWF mutants, although rarely for p.Cys1060Tyr (Figure 3).

Impaired WPB formation and increased intracellular retention

We randomly selected confocal microscopy fields and analyzed 150~300 cells from each sample for the quantification of VWF storage patterns. First, we analyzed the formation of pseudo-WPB per se following expression of WT-VWF or VWF variants. The proportion of cells containing more than 30 pseudo-WPB per cell was over 70% in WT-VWF transfected cells, which was much higher than for the VWF variants (Figure 4A).

To further characterize the effects of the mutations on the elongation of pseudo-WPB, cells were categorized according to the number of elongated pseudo-WPB per cell. The proportion of cells containing more than 4 elongated pseudo-WPB was decreased for all mutants (Figure 4B). Interestingly, the number of pseudo-WPB formed by p.Cys1060Tyr per cell was comparable to p.Cys2754Trp (Figure 4A), but the proportion of cells containing more than 4 elongated pseudo-WPB was much lower for the latter (68% for p.Cys1060Tyr versus 18% for p.Cys2754Trp), indicating that the majority of the pseudo-WPB formed by p.Cys2754Trp were rather round (Figure 4B). Upon co-transfection with WT-VWF, the defects in the number and elongation of the pseudo-WPB caused by the mutations were partly corrected (Figure 4C-D).

Finally, the retention of VWF variants in the ER was quantified. As shown in Figure 5, only a small population of cells expressing WT-VWF (less than 10%) showed that part of the VWF was located in the ER, which may be due to protein overexpression in HEK293 cells. The proportion of cells with VWF located in the ER was slightly increased by p.Cys1060Tyr compared to that by WT-VWF, whereas it was drastically increased by p.Cys1149Arg, p.Cys2739Tyr and p.Cys2754Trp. It indicates the latter three mutations caused a marked retention of VWF in the ER with less VWF stored in the pseudo-WPB (Figure 5B).

The defects in VWF storage caused by the mutations were a net effect of impaired pseudo-WPB formation, lack of elongation of pseudo-WPB, and increased ER retention of VWF. All three aspects were corrected to different extents by co-transfection of these variants with WT-VWF (Figures 4C-D and 5C).

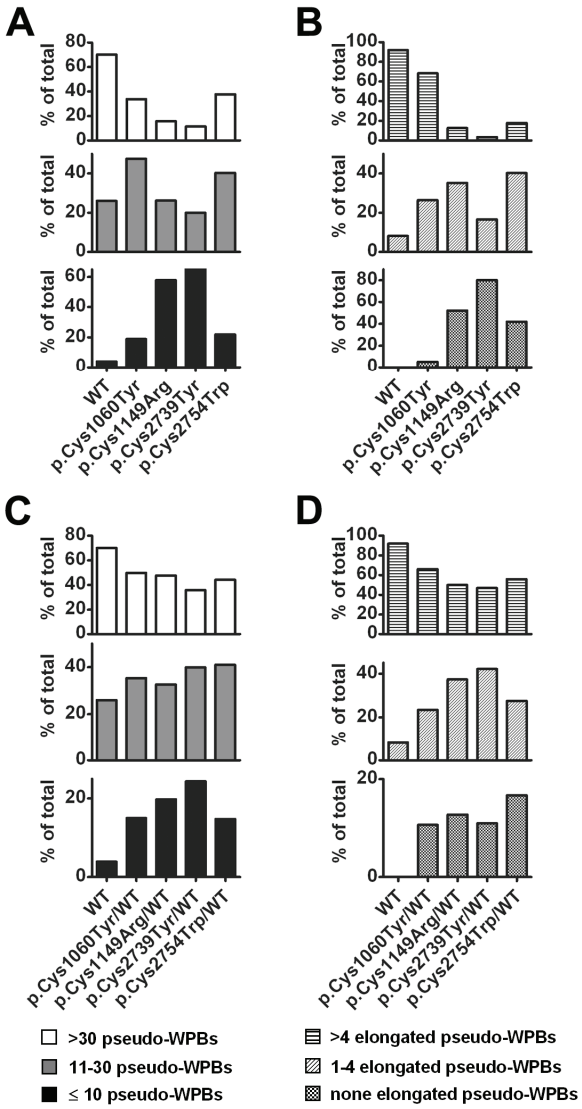

Figure 4. Defects in the pseudo-WPB formation. Transfected HEK293 cells were fixed and stained as described in Figure 2, 72 hours after the single transfection (A, B) or co-transfection (C, D). Images were randomly taken by the confocal microscopy and all transfected cells in the images were selected for quantitative analysis. The selected cells were divided into three categories according to the number of pseudo-WPB per cell (A, C): more than 30; from 11 to 30; fewer than 10 pseudo-WPB per cell; or according to the number of elongated pseudo-WPB per cell (B, D): more than 4; from 1 to 4; none elongated pseudo-WPB per cell. The graph represents the percentage of cells in each category. 150~300 cells expressing VWF variants were analyzed for each bar. Each bar represents the mean of 2 independent experiments.

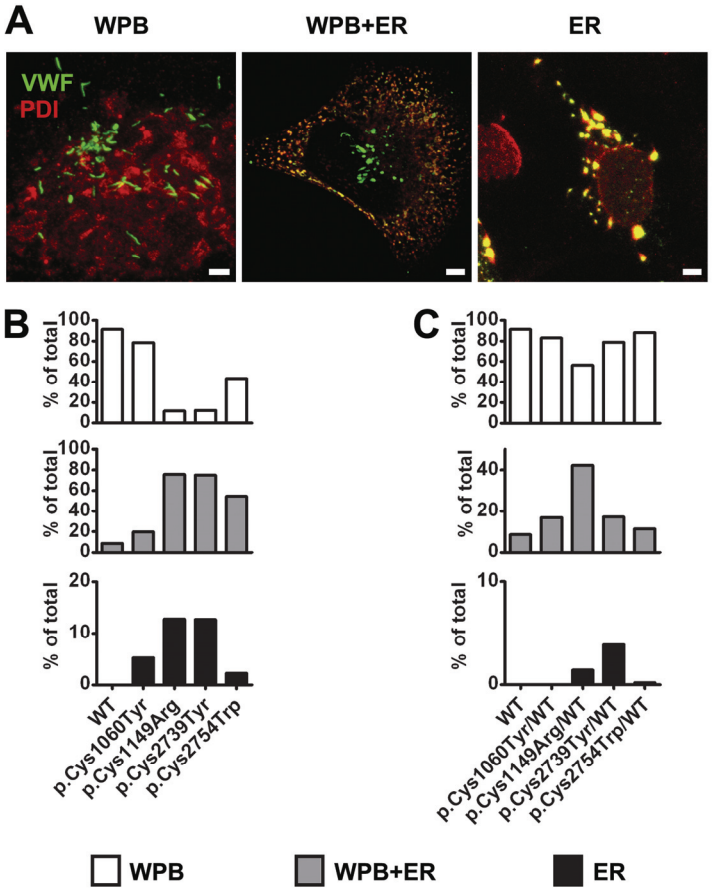

Figure 5. Retention of VWF in the ER. According to the intracellular location of VWF in transfected HEK293 cells, the selected cells were classified into 3 categories (A): "WPB" represents cells with all intracellular VWF stored in pseudo-WPB (green); "WPB+ER" represents cells with intracellular VWF located in both ER (yellow) and pseudo-WPB (green); and "ER" represents cells with all intracellular VWF located in ER (yellow). Scale bars = 5 µm. (B, C) The graph represents the percentage of cells in each category. 150~300 cells expressing VWF variants were analyzed for each bar. Each bar represents the mean of 2 independent experiments.

Regulated secretion of VWF

Release of pseudo-WPB from HEK293 cells can be induced by secretagogues such as PMA [17]. Incubation of HEK293 cells for 60 minutes with PMA increased the secretion of WT-VWF from 4.3% (Ctr) to 10.5% (+PMA), a 2.4 times increase (Figure 6). The induced secretion under stimulation was slightly lower with

p.Cys1060Tyr, but much less with the other three mutations. No detectable induced release was observed by stimulation of p.Cys1149Arg or p.Cys2739Tyr transfected cells. In co-transfections of all four variants with WT-VWF at a 1:1 ratio, PMA stimulation resulted in a 2.5 to 3.1 times increase of secretion over unstimulated cells, comparable to WT-VWF. However, the percentage of total VWF that was secreted, basal (Ctr) as well as stimulated (+PMA), was only partly restored in co-transfections of p.Cys1149Arg.

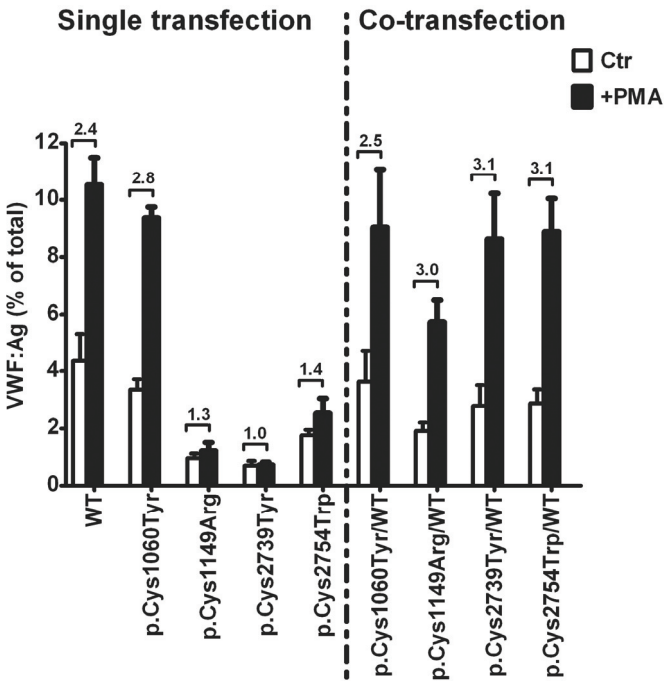

Figure 6. Effects of quantitative mutations on the regulated secretion of VWF. Seventy-two hours post transfection, HEK293 cells were rinsed twice with the release medium and incubated at 37°C for 60 minutes in the release medium without (Ctr) or with 160 nM PMA (+PMA). Then the release media and cell lysates were collected as described in the methods. Each bar represents VWF secreted into the release medium as a fraction of total VWF (secreted plus intracellular) ± SEM (three independent experiments in duplicate). The numbers above the bars indicate the fold increase of secreted VWF comparing the stimulated (+PMA) and control (Ctr) samples.

Multimeric analysis of VWF

The full range of VWF multimers was present in both the conditioned medium and the lysate of WT-VWF transfected HEK293 cells (Figure 7A-B). The pattern was comparable to the multimers obtained from HUVECs (Figure 7B), confirming the validity of the HEK293 system for the study of synthesis and storage of HMW multimers.

Compared to WT-VWF, p.Cys1060Tyr led to the loss of the largest multimers in secreted VWF (Figure 7A). p.Cys1149Arg and p.Cys2754Trp showed more severe defects in the VWF multimerization with mainly dimers for p.Cys1149Arg and abundant monomers and dimers as well as additional trimers and tetramers for p.Cys2754Trp. The VWF levels in media were too low to visualize multimers for p.Cys2739Tyr (Figure 7A). The multimer patterns of VWF in the lysates were comparable to the patterns in conditioned media for all the VWF variants, except for p.Cys2739Tyr which could not be visualized in medium and showed mainly monomers in the cell lysate (Figure 7B).

Co-transfection of each of the variants with WT-VWF yielded a wide range of multimers (Figure 7C-D). Interestingly, p.Cys2754Trp/WT-VWF yielded additional odd-numbered multimers in the medium (Figure 7C). As shown before, trimers and higher odd-numbered multimers in p.Cys2754Trp result from N-terminal disulfide bond formation of the excess of monomers [40]. The appearance of the larger odd-numbered multimers is clear evidence for the actual formation of heterodimers and heteromultimers in the co-transfections.

To confirm correct processing of VWF in HEK293 cells, we performed reducing SDS-PAGE. The secreted VWF is mainly mature VWF, while in the cell lysates mature VWF as well as uncleaved proVWF was shown for WT-VWF and p.Cys1060Tyr (Figure 7E). The other mutants showed primarily uncleaved proVWF in the cell lysates (Figure 7E). This is consistent with the observation that VWF is mainly stored in pseudo-WPB for WT-VWF and p.Cys1060Tyr but retained in the ER for the other three mutants (Figure 5B).

Discussion

In this study we analyzed the intracellular storage and regulated secretion of VWF. Our findings highlight the detailed effects of VWF mutations on the formation of WPB and on the basal and regulated secretion of VWF. Through these mechanisms the pathogenic nature of those mutations in VWD are unraveled.

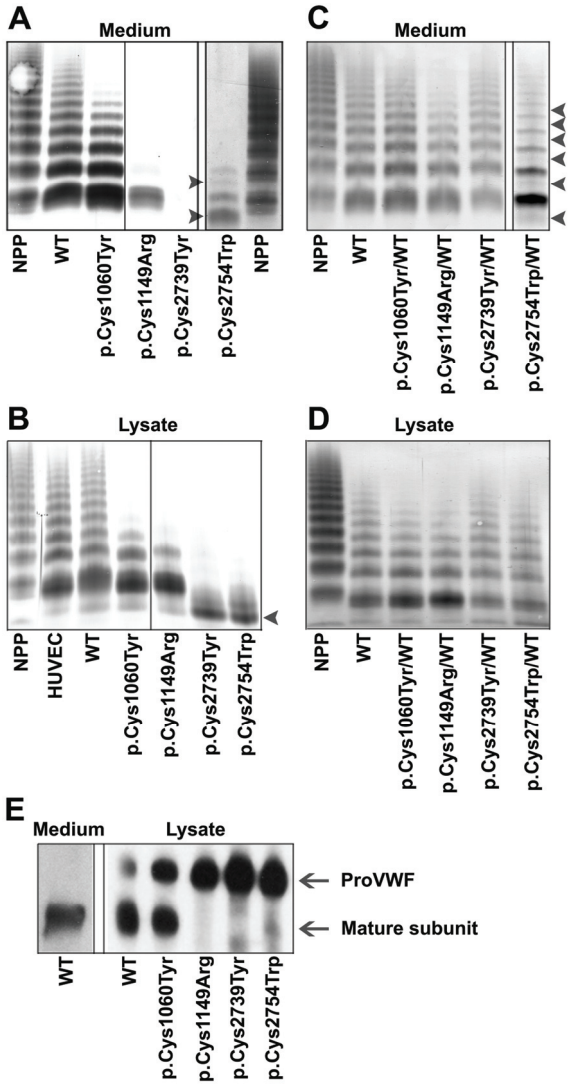

Figure 7. Electrophoretic characteristics of VWF in the media and lysates. Seventy-two hours after the single transfection (A, B, E) or co-transfection (C, D), HEK293 cells were rinsed and incubated with the release medium at 37°C. After 24 hours media (A, C) and lysates (B, D) were collected and analyzed under non-reducing conditions. Normal pooled plasma (NPP) was used as control for the multimer analysis. The arrowheads in panels A, B and C indicate the odd-numbered multimers. In panels A and B the parts separated by the line between p.Cys1060Tyr and p.Cys1149Arg were from the same gel. In panels A and C, the lanes for p.Cys2754Trp are from another experiment showing more clearly the odd-numbered multimers. In panel E, VWF was analyzed under reducing conditions. Lanes 1 (from a different gel) and 2 show WT-VWF in the conditioned medium and lysate, respectively; lanes 3-6 show p.Cys1060Tyr, p.Cys1149Arg, p.Cys2739Tyr and p.Cys2754Trp in the lysate, respectively.

Due to the lack of WPB formation in most expression systems that have been extensively applied [21,41], the current concept of the pathogenesis of VWF mutations identified in VWD are mainly based on the expression data on the constitutive secretion, synthesis and multimer patterns of VWF. However, the main source of VWF in the circulation is the endothelial cells that synthesize and store VWF into WPB and secrete VWF into the circulation through basal and regulated pathways [8,9]. We therefore believe that the analysis of VWF mutations in an expression system, like HEK293 cells, that can form WPB like storage organelles will yield additional insight into the pathogenic nature of VWF mutations [17].

We confirmed the validity of the HEK293 cell model. Upon expression of WT-VWF the HEK293 cells formed intracellular storage organelles, pseudo-WPB, which were indistinguishable from endothelial WPB. Furthermore, these pseudo-WPB stored multimeric VWF, displayed an elongated shape with a size of 100~200 nm by 1~5 µm, contained internal striations representing VWF tubules, and actively secreted stored VWF upon PMA-stimulation. By expression of the four VWF mutants in HEK293 cells, we found that intracellular accumulation of VWF mutants was associated with ER retention, dilation of the ER, and disturbed WPB formation (fewer and morphologically abnormal pseudo-WPB). These defects in VWF routing were accompanied by reduced basal and regulated secretion. The combined effects are summarized in Table 2.

The ER retention and dilated ER are most likely caused by the VWF mutations *per se* as dilated ER was neither observed in mock-transfected cells nor in cells expressing WT-VWF (Figure 3). Dilated ER is unlikely to be the result of delayed exiting of mutant VWF from the ER, as prolonged culturing of cells after transient transfection for 72 hours, or even for a much longer period of up to 6 days for stably transfected cells, did not result in reduction of ER retention nor in more pseudo-WPB formation (supplemental Figure S2).

The retention of VWF mutants in the ER also impaired storage into WPB and trafficking of VWF into the regulated secretion pathway. Compared with WT-VWF, the mutations strongly decreased the number of pseudo-WPB (p.Cys1149Arg and p.Cys2739Tyr) as well as the length of these organelles (p.Cys1149Arg, p.Cys2739Tyr and p.Cys2754Trp) (Figure 4 and Table 2). Diminished post-Golgi storage of these mutants was also confirmed by the presence of abundant uncleaved proVWF in the cell lysates (Figure 7E). Since pseudo-WPB resemble endothelial WPB and likely serve as the releasable pool of VWF upon stimulation [11,17], decrease in the size of this releasable pool caused by the VWF mutations

Table 2. Summary of defects caused by VWF mutants as compared to WT-VWF

Domain	*Variant*	*VWD type*	*ER retention*	*Pseudo-WPB formation*			*Secretion of VWF*		*Secreted multimers*
				No.	Elongated shape§	Tubular storage‖	Basal	Stimulated	
D3	p.Cys1060Tyr	1*	↑	↓	↓	Normal	↓	Normal/↓	Lack of HMW multimers
CK	p.Cys2754Trp	3†	↑↑	↓	↓↓	Severely affected	↓↓	↓↓	Mainly LMW multimers¶
D3	p.Cys1149Arg	1*	↑↑↑	↓↓↓	↓↓	Normal but shorter	↓↓↓	↓↓↓	Mainly dimers
CK	p.Cys2739Tyr	3‡	↑↑↑	↓↓↓	↓↓↓	Not confirmed	↓↓↓	↓↓↓	Not detectable

*patient heterozygous

†patient homozygous

‡patient compound heterozygous for a premature stop codon on the other allele

§based on the immunofluorescent analysis

‖based on the TEM analysis

¶showed odd-numbered multimers

explains the attenuated regulated secretion of VWF (Figure 6 and Table 2). The impaired elongation of pseudo-WPB may also attenuate the regulated secretion of VWF. It has been shown that rounding of WPB by disturbing intracellular pH environment with monensin does not affect the regulated secretion of VWF [18], however, the effects of the disturbance in elongation of WPB by specific mutations of VWF are currently unclear. We speculate that round shaped WPB caused by VWF mutations may be functionally different from the shape changes induced by modulation of intra-organellular pH.

We observed that a substantial number of pseudo-WPB formed by p.Cys1149Arg were shorter and/or round (Figures 2D, 2Fii-ii", 4C and supplemental Figure S2). The short pseudo-WPB may reflect the formation of shorter or less rigid VWF tubules by this mutant. VWF p.Cys1149Arg might have disrupted tubulation and storage of VWF in the cells due to the decreased binding of mature VWF p.Cys1149Arg to the propeptide [42], which has been shown to be essential for the unique storage of VWF in compacted tubules, resulting in the elongated shape of WPB [18,19].

The elongation of WPB depends on the correct tubulation of VWF. Expression of truncated VWF constructs has shown that the D1D2D'D3A1 domains are sufficient to form elongated pseudo-WPB [18] and the remaining part of VWF is supposed to form the matrix between tubules [19]. In this study, we found that two natural mutations in the CK domain of VWF, p.Cys2739Tyr and p.Cys2754Trp, severely disturbed the elongation of pseudo-WPB. In particular, p.Cys2754Trp formed numerous round pseudo-WPB (93% of total pseudo-WPB observed by TEM) with tubules in disarray (Figure 2E, 2Fi-i" and supplemental Figure S1C). The defects in elongation of these pseudo-WPB may be partially due to relatively low concentrations of these variants available for tubulation in the *trans*-Golgi network as abundant VWF was retained in the ER (Figures 1D-E, 3E-F and 5B). The round pseudo-WPB in p.Cys2754Trp transfected cells are not just explained by immaturity of pseudo-WPB as immature pseudo-WPB in WT-VWF transfected cells showed regular and parallel tubules (supplemental Figure S1A-B). Interestingly, round pseudo-WPB formed by p.Cys2754Trp showed disorganized storage of VWF tubules, which were different from the transversely cut WPB [38,43,44] or VWF subunit-containing structures [44]. The disordered VWF tubules suggest that p.Cys2754Trp deteriorates the matrix between VWF tubules, and further disturbs the rigidity of VWF tubules. As proposed, the rigidity of VWF tubules is responsible for the elongation of WPB [45], therefore, we argue that disturbance of the matrix

by mutations in the CK domain, in addition to the D1D2D'D3A1 domains, might also limit the length of WPB.

HMW VWF multimers are released from WPB at sites of vascular damage in response to secretion stimuli like thrombin, stress, vasopressin or its synthetic analogue desmopressin (DDAVP), which is used in the treatment of VWD. The formation and exocytosis of WPB are therefore important in determining the VWD phenotype as well as treatment. The expression data predict that patients heterozygous for p.Cys1060Tyr or p.Cys1149Arg (mimicked by co-transfections with WT-VWF) have a mild reduction in numbers of endothelial WPB and an intermediate response to DDAVP [46], whereas the patients who are compound heterozygous for p.Cys2739Tyr or homozygous for p.Cys2754Trp will have severely reduced numbers and aberrant WPB and will display a poor response to DDAVP. The VWF level detected in the medium in co-transfections is higher than may be expected based on the plasma VWF:Ag levels observed in the patients, but this is explained by the fact that in the expression system there is no contribution of clearance. Increased clearance has been implicated in several type 1 VWD patients before and specifically has been shown for p.Cys1149Arg [42]. The increased clearance contributes to the dominant-negative effects of the mutations.

As shown in other expression systems [20,23,47], missense mutations in VWF lead to a structural change of the protein which may result in multimer abnormality in single-transfections as seen in the present study. However, the range of VWF multimers in the type 1 VWD patients heterozygous for p.Cys1060Tyr and p.Cys1149Arg, respectively, was recapitulated in the co-transfections with only a marginal decrease of the largest multimers that mimic the heterozygous states in the patients (Figure 7C). Mutations p.Cys2739Tyr and p.Cys2754Trp are known to disrupt the dimerization of VWF and result in abnormal multimerization [23], while the extremely low levels of VWF secretion corresponded to the phenotype of VWD type 3 patients [32,33]. Thus, even though the single transfections show abnormalities at the multimer level, the main effect of the mutations on the phenotype is quantitative.

In conclusion, our results show that disrupted trafficking of VWF to WPB (and/or formation of aberrant WPB) and consequently a decreased regulated secretion of VWF is a potentially common pathogenic mechanism in some VWD subtypes with quantitative deficiencies of VWF. Although we have focused on mutations involving cysteines, also non-cysteine mutations may be implicated in similar mechanisms as was suggested for p.Arg273Trp [17] and p.Arg854Trp [48]. Accompanying effects

on WPB secretion and VWF string formation may also contribute to the clinical phenotype, and therefore the effects of VWF mutations on these aspects need further study. Analysis of the WPB formation and function can be a promising way to evaluate the pathogenic nature of VWF mutations and may bring more new insights into the mechanisms underlying VWD.

Acknowledgements

This work was financially supported by a grant from the China Scholarship Council (2007U21083) and partially by a grant from the Netherlands Organisation for Scientific Research (NWO), grant no. 91209006.

We thank from the Department of Molecular Cell Biology, Leiden University of Medical Center, Erik Bos, Karen A. Jansen, Jos J.M. Onderwater, Frank Faas, Jan C.M. Slats, Annelies van der Laan for expert technical assistance and Jack A. Valentijn for helpful discussion and help with the confocal imaging. We thank Hans Vos from the Department of Thrombosis and Hemostasis for helpful suggestions to make plasmids. We thank Annemarie van Oeveren-Rietdijk from the Department of Nephrology, Leiden University of Medical Center, for providing the HUVECs.

References

1. Sadler JE. Biochemistry and genetics of von Willebrand factor. *Annu Rev Biochem* 1998; **67**:395-424.
2. Sadler JE, Budde U, Eikenboom JC, Favaloro EJ, Hill FG, Holmberg L, Ingerslev J, Lee CA, Lillicrap D, Mannucci PM, Mazurier C, Meyer D, Nichols WL, Nishino M, Peake IR, Rodeghiero F, Schneppenheim R, Ruggeri ZM, Srivastava A, Montgomery RR, Federici AB. Update on the pathophysiology and classification of von Willebrand disease: a report of the Subcommittee on von Willebrand Factor. *J Thromb Haemost* 2006; **4**:2103-2114.
3. Cumming A, Grundy P, Keeney S, Lester W, Enayat S, Guilliatt A, Bowen D, Pasi J, Keeling D, Hill F, Bolton-Maggs PH, Hay C, Collins P. An investigation of the von Willebrand factor genotype in UK patients diagnosed to have type 1 von Willebrand disease. *Thromb Haemost* 2006; **96**:630-641.
4. Goodeve A, Eikenboom J, Castaman G, Rodeghiero F, Federici AB, Batlle J, Meyer D, Mazurier C, Goudemand J, Schneppenheim R, Budde U, Ingerslev J, Habart D, Vorlova Z, Holmberg L, Lethagen S, Pasi J, Hill F, Hashemi SM, Baronciani L, Hallden C, Guilliatt A, Lester W, Peake I. Phenotype and genotype of a cohort of families historically diagnosed with type 1 von Willebrand disease in the European study, Molecular and Clinical Markers for the Diagnosis and Management of Type 1 von Willebrand Disease (MCMDM-1VWD). *Blood* 2007; **109**:112-121.
5. James PD, Notley C, Hegadorn C, Leggo J, Tuttle A, Tinlin S, Brown C, Andrews C, Labelle A, Chirinian Y, O'Brien L, Othman M, Rivard G, Rapson D, Hough C, Lillicrap D. The

mutational spectrum of type 1 von Willebrand disease: Results from a Canadian cohort study. *Blood* 2007; **109**:145-154.

6. Eikenboom JC. Congenital von Willebrand disease type 3: clinical manifestations, pathophysiology and molecular biology. *Best Pract Res Clin Haematol* 2001; **14**:365-379.
7. Verweij CL, Diergaarde PJ, Hart M, Pannekoek H. Full-length von Willebrand factor (vWF) cDNA encodes a highly repetitive protein considerably larger than the mature vWF subunit. *EMBO J* 1986; **5**:1839-1847.
8. Mayadas T, Wagner DD, Simpson PJ. von Willebrand factor biosynthesis and partitioning between constitutive and regulated pathways of secretion after thrombin stimulation. *Blood* 1989; **73**:706-711.
9. Giblin JP, Hewlett LJ, Hannah MJ. Basal secretion of von Willebrand factor from human endothelial cells. *Blood* 2008; **112**:957-964.
10. Dong JF, Moake JL, Nolasco L, Bernardo A, Arceneaux W, Shrimpton CN, Schade AJ, McIntire LV, Fujikawa K, Lopez JA. ADAMTS-13 rapidly cleaves newly secreted ultralarge von Willebrand factor multimers on the endothelial surface under flowing conditions. *Blood* 2002; **100**:4033-4039.
11. Sporn LA, Marder VJ, Wagner DD. Inducible secretion of large, biologically potent von Willebrand factor multimers. *Cell* 1986; **46**:185-190.
12. Sporn LA, Marder VJ, Wagner DD. von Willebrand factor released from Weibel-Palade bodies binds more avidly to extracellular matrix than that secreted constitutively. *Blood* 1987; **69**:1531-1534.
13. Ewenstein BM, Warhol MJ, Handin RI, Pober JS. Composition of the von Willebrand factor storage organelle (Weibel-Palade body) isolated from cultured human umbilical vein endothelial cells. *J Cell Biol* 1987; **104**:1423-1433.
14. Hop C, Guilliatt A, Daly M, de Leeuw HP, Brinkman HJ, Peake IR, van Mourik JA, Pannekoek H. Assembly of multimeric von Willebrand factor directs sorting of P-selectin. *Arterioscler Thromb Vasc Biol* 2000; **20**:1763-1768.
15. Voorberg J, Fontijn R, Calafat J, Janssen H, van Mourik JA, Pannekoek H. Biogenesis of von Willebrand factor-containing organelles in heterologous transfected CV-1 cells. *EMBO J* 1993; **12**:749-758.
16. Wagner DD, Saffaripour S, Bonfanti R, Sadler JE, Cramer EM, Chapman B, Mayadas TN. Induction of specific storage organelles by von Willebrand factor propolypeptide. *Cell* 1991; **64**:403-413.
17. Michaux G, Hewlett LJ, Messenger SL, Goodeve AC, Peake IR, Daly ME, Cutler DF. Analysis of intracellular storage and regulated secretion of 3 von Willebrand disease-causing variants of von Willebrand factor. *Blood* 2003; **102**:2452-2458.
18. Michaux G, Abbitt KB, Collinson LM, Haberichter SL, Norman KE, Cutler DF. The physiological function of von Willebrand's factor depends on its tubular storage in endothelial Weibel-Palade bodies. *Dev Cell* 2006; **10**:223-232.
19. Huang RH, Wang Y, Roth R, Yu X, Purvis AR, Heuser JE, Egelman EH, Sadler JE. Assembly of Weibel-Palade body-like tubules from N-terminal domains of von Willebrand factor. *Proc Natl Acad Sci U S A* 2008; **105**:482-487.
20. Eikenboom JC, Matsushita T, Reitsma PH, Tuley EA, Castaman G, Briet E, Sadler JE. Dominant type 1 von Willebrand disease caused by mutated cysteine residues in the D3 domain of von Willebrand factor. *Blood* 1996; **88**:2433-2441.

21. Eikenboom J, Hilbert L, Ribba AS, Hommais A, Habart D, Messenger S, Al-Buhairan A, Guilliatt A, Lester W, Mazurier C, Meyer D, Fressinaud E, Budde U, Will K, Schneppenheim R, Obser T, Marggraf O, Eckert E, Castaman G, Rodeghiero F, Federici AB, Batlle J, Goudemand J, Ingerslev J, Lethagen S, Hill F, Peake I, Goodeve A. Expression of 14 von Willebrand factor mutations identified in patients with type 1 von Willebrand disease from the MCMDM-1VWD study. *J Thromb Haemost* 2009; **7**:1304-1312.
22. Tjernberg P, Castaman G, Vos HL, Bertina RM, Eikenboom JC. Homozygous C2362F von Willebrand factor induces intracellular retention of mutant von Willebrand factor resulting in autosomal recessive severe von Willebrand disease. *Br J Haematol* 2006; **133**:409-418.
23. Tjernberg P, Vos HL, Castaman G, Bertina RM, Eikenboom JC. Dimerization and multimerization defects of von Willebrand factor due to mutated cysteine residues. *J Thromb Haemost* 2004; **2**:257-265.
24. Allen S, Abuzenadah AM, Hinks J, Blagg JL, Gursel T, Ingerslev J, Goodeve AC, Peake IR, Daly ME. A novel von Willebrand disease-causing mutation (Arg273Trp) in the von Willebrand factor propeptide that results in defective multimerization and secretion. *Blood* 2000; **96**:560-568.
25. Allen S, Abuzenadah AM, Blagg JL, Hinks J, Nesbitt IM, Goodeve AC, Gursel T, Ingerslev J, Peake IR, Daly ME. Two novel type 2N von Willebrand disease-causing mutations that result in defective factor VIII binding, multimerization, and secretion of von Willebrand factor. *Blood* 2000; **95**:2000-2007.
26. Casonato A, Cattini MG, Soldera C, Marcato S, Sartorello F, Pontara E, Pagnan A. A new L1446P mutation is responsible for impaired von Willebrand factor synthesis, structure, and function. *J Lab Clin Med* 2004; **144**:254-259.
27. Casonato A, Sartorello F, Cattini MG, Pontara E, Soldera C, Bertomoro A, Girolami A. An Arg760Cys mutation in the consensus sequence of the von Willebrand factor propeptide cleavage site is responsible for a new von Willebrand disease variant. *Blood* 2003; **101**:151-156.
28. Casonato A, Sartorello F, Pontara E, Gallinaro L, Bertomoro A, Grazia CM, Daidone V, Szukowska M, Pagnan A. A novel von Willebrand factor mutation (I1372S) associated with type 2B-like von Willebrand disease: an elusive phenotype and a difficult diagnosis. *Thromb Haemost* 2007; **98**:1182-1187.
29. Hommais A, Stepanian A, Fressinaud E, Mazurier C, Meyer D, Girma JP, Ribba AS. Mutations C1157F and C1234W of von Willebrand factor cause intracellular retention with defective multimerization and secretion. *J Thromb Haemost* 2006; **4**:148-157.
30. Rosenberg JB, Haberichter SL, Jozwiak MA, Vokac EA, Kroner PA, Fahs SA, Kawai Y, Montgomery RR. The role of the D1 domain of the von Willebrand factor propeptide in multimerization of VWF. *Blood* 2002; **100**:1699-1706.
31. Hampshire DJ, Burghel GJ, Goudemand J, Bouvet LC, Eikenboom JC, Schneppenheim R, Budde U, Peake IR, Goodeve AC. Polymorphic variation within the VWF gene contributes to the failure to detect mutations in patients historically diagnosed with type 1 VWD from the MCMDM-1VWD cohort. *Haematologica* 2010; **95**:2163-2165.
32. Zhang ZP, Blomback M, Egberg N, Falk G, Anvret M. Characterization of the von Willebrand factor gene (VWF) in von Willebrand disease type III patients from 24 families of Swedish and Finnish origin. *Genomics* 1994; **21**:188-193.

33. Schneppenheim R, Budde U, Obser T, Brassard J, Mainusch K, Ruggeri ZM, Schneppenheim S, Schwaab R, Oldenburg J. Expression and characterization of von Willebrand factor dimerization defects in different types of von Willebrand disease. *Blood* 2001; **97**:2059-2066.
34. Jaffe EA, Nachman RL, Becker CG, Minick CR. Culture of human endothelial cells derived from umbilical veins. Identification by morphologic and immunologic criteria. *J Clin Invest* 1973; **52**:2745-2756.
35. Romani de WT, Rondaij MG, Hordijk PL, Voorberg J, van Mourik JA. Real-time imaging of the dynamics and secretory behavior of Weibel-Palade bodies. *Arterioscler Thromb Vasc Biol* 2003; **23**:755-761.
36. Benham AM, Cabibbo A, Fassio A, Bulleid N, Sitia R, Braakman I. The CXXCXXC motif determines the folding, structure and stability of human Ero1-Lalpha. *EMBO J* 2000; **19**:4493-4502.
37. Mommaas AM, Mulder AA, Out CJ, Girolomoni G, Koerten HK, Vermeer BJ, Koning F. Distribution of HLA class II molecules in epidermal Langerhans cells in situ. *Eur J Immunol* 1995; **25**:520-525.
38. Valentijn KM, Valentijn JA, Jansen KA, Koster AJ. A new look at Weibel-Palade body structure in endothelial cells using electron tomography. *J Struct Biol* 2008; **161**:447-458.
39. Bodo I, Katsumi A, Tuley EA, Eikenboom JC, Dong Z, Sadler JE. Type 1 von Willebrand disease mutation Cys1149Arg causes intracellular retention and degradation of heterodimers: a possible general mechanism for dominant mutations of oligomeric proteins. *Blood* 2001; **98**:2973-2979.
40. Tjernberg P, Vos HL, Spaargaren-van Riel CC, Luken BM, Voorberg J, Bertina RM, Eikenboom JC. Differential effects of the loss of intrachain- versus interchain-disulfide bonds in the cystine-knot domain of von Willebrand factor on the clinical phenotype of von Willebrand disease. *Thromb Haemost* 2006; **96**:717-724.
41. Wang JW, Eikenboom J. Von Willebrand disease and Weibel-Palade bodies. *Hamostaseologie* 2010; **30**:150-155.
42. Schooten CJ, Tjernberg P, Westein E, Terraube V, Castaman G, Mourik JA, Hollestelle MJ, Vos HL, Bertina RM, Berg HM, Eikenboom JC, Lenting PJ, Denis CV. Cysteine-mutations in von Willebrand factor associated with increased clearance. *J Thromb Haemost* 2005; **3**:2228-2237.
43. Lui-Roberts WW, Collinson LM, Hewlett LJ, Michaux G, Cutler DF. An AP-1/clathrin coat plays a novel and essential role in forming the Weibel-Palade bodies of endothelial cells. *J Cell Biol* 2005; **170**:627-636.
44. Zenner HL, Collinson LM, Michaux G, Cutler DF. High-pressure freezing provides insights into Weibel-Palade body biogenesis. *J Cell Sci* 2007; **120**:2117-2125.
45. Berriman JA, Li S, Hewlett LJ, Wasilewski S, Kiskin FN, Carter T, Hannah MJ, Rosenthal PB. Structural organization of Weibel-Palade bodies revealed by cryo-EM of vitrified endothelial cells. *Proc Natl Acad Sci U S A* 2009; **106**:17407-17412.
46. Federici AB. The use of desmopressin in von Willebrand disease: the experience of the first 30 years (1977-2007). *Haemophilia* 2008; **14 Suppl 1**:5-14.
47. Schneppenheim R, Michiels JJ, Obser T, Oyen F, Pieconka A, Schneppenheim S, Will K, Zieger B, Budde U. A cluster of mutations in the D3 domain of von Willebrand factor correlates with a distinct subgroup of von Willebrand disease: type 2A/IIE. *Blood* 2010; **115**:4894-4901.

48. Castaman G, Giacomelli SH, Jacobi P, Obser T, Budde U, Rodeghiero F, Haberichter SL, Schneppenheim R. Homozygous type 2N R854W von Willebrand factor is poorly secreted and causes a severe von Willebrand disease phenotype. *J Thromb Haemost* 2010; **8**:2011-2016.

Supplemental data

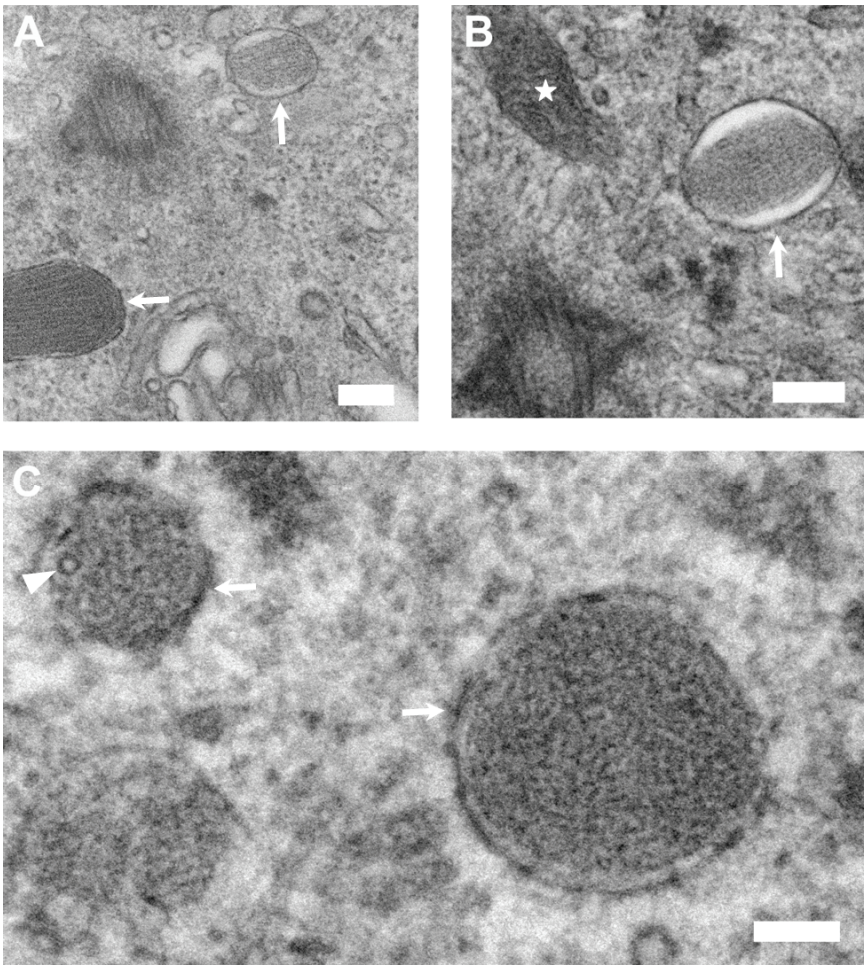

Figure S1. Round pseudo-WPBs observed by TEM. HEK293 cells were fixed 72 hours post transfection with WT-VWF (A-B) or p.Cys2754Trp (C) and analyzed with TEM. Panel A shows one elongated pseudo-WPB (lower left) and one round pseudo-WPB (upper right). Panel B shows one similar round pseudo-WPB observed in a different cell expressing WT-VWF. Panel C shows two round pseudo-WPBs formed by p.Cys2754Trp. Note the difference of the round pseudo-WPBs formed by WT-VWF and p.Cys2754Trp: VWF tubules were stored longitudinally like those in the elongated pseudo-WPB (panel A, lower left) for WT-VWF, but in disarray for p.Cys2754Trp. The arrowhead indicates a transverse tubule (panel C). The arrows and star indicate the pseudo-WPBs and mitochondrion, respectively. Scale bars = 200 nm. All electron micrographs were acquired with a FEI Tecnai 12 TEM at 120 kV and using an FEI Eagle 4kx4k CCD camera.

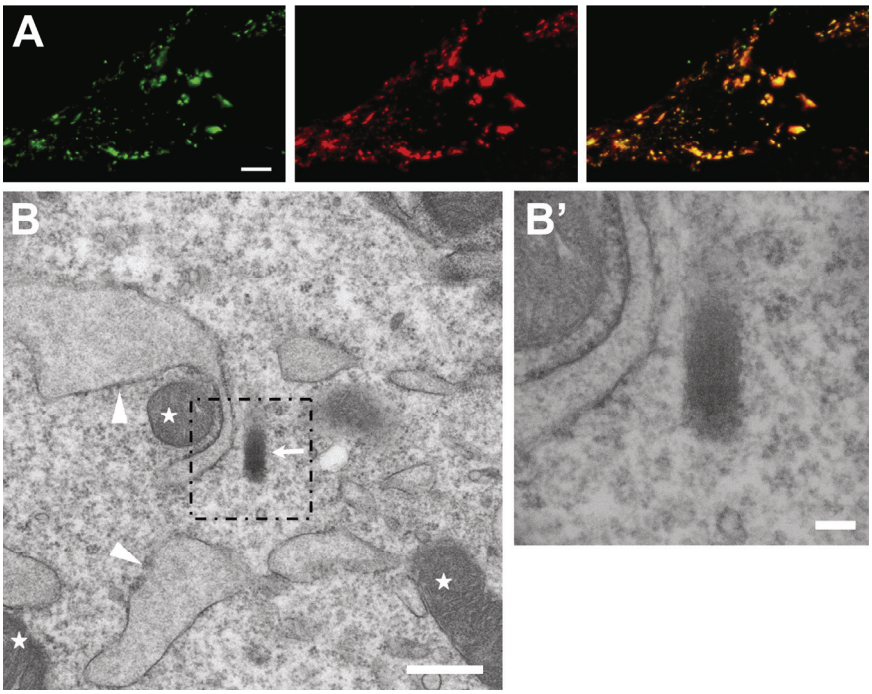

Figure S2. Defects in VWF storage in stable cell line expressing p.Cys1149Arg. (A) HEK293 cells stably expressing p.Cys1149Arg were fixed and stained for VWF (green channel) and PDI (red channel). The double staining was detected in the yellow merged colors (right panel). The overlapping of VWF and PDI (yellow) indicates that the majority of p.Cys1149Arg is retained in the ER. Scale bar = 5 µm. (B) HEK293 cells stably expressing p.Cys1149Arg were fixed and prepared for TEM. The figure shows the presence of pseudo-WPB and dilated ER together in the same cell. The arrow, arrowheads and stars indicate the pseudo-WPBs, ER and mitochondria, respectively. Scale bar = 500 nm. (B') Higher magnification TEM view of the pseudo-WPB in the boxed area in B. Scale bar = 100 nm. The immunofluorescence images were acquired with a Leica SL confocal laser-scanning microscopy, using a 63X oil immersion objective with a numerical aperture of 1.40 (Leica HCX PL APO). The electron micrograph was acquired with a FEI Tecnai 12 TEM at 120 kV and using an FEI Eagle 4kx4k CCD camera.